Stem Cell Reports
Article

ISSCR

OPEN ACCESS

Non-monotonic Changes in Progenitor Cell Behavior and Gene Expression during Aging of the Adult V-SVZ Neural Stem Cell Niche

Maria Apostolopoulou,[1] Thomas R. Kiehl,[1,*] Mark Winter,[2] Edgar Cardenas De La Hoz,[2] Nathan C. Boles,[1] Christopher S. Bjornsson,[1] Kristen L. Zuloaga,[1,3] Susan K. Goderie,[1] Yue Wang,[1] Andrew R. Cohen,[2] and Sally Temple[1,*]

[1]Neural Stem Cell Institute, Rensselaer, NY 12144, USA
[2]Electrical and Computer Engineering, Drexel University, Philadelphia, PA 19104, USA
[3]Department of Neuroscience and Experimental Therapeutics, Albany Medical College, Albany, NY 12208, USA
*Correspondence: sallytemple@neuralsci.org (S.T.), tomkiehl@neuralsci.org (T.R.K.)
https://doi.org/10.1016/j.stemcr.2017.10.005

SUMMARY

Neural stem cell activity in the ventricular-subventricular zone (V-SVZ) decreases with aging, thought to occur by a unidirectional decline. However, by analyzing the V-SVZ transcriptome of male mice at 2, 6, 18, and 22 months, we found that most of the genes that change significantly over time show a reversal of trend, with a maximum or minimum expression at 18 months. *In vivo*, MASH1$^+$ progenitor cells decreased in number and proliferation between 2 and 18 months but increased between 18 and 22 months. Time-lapse lineage analysis of 944 V-SVZ cells showed that age-related declines in neurogenesis were recapitulated *in vitro* in clones. However, activated type B/type C cell clones divide slower at 2 to 18 months, then unexpectedly faster at 22 months, with impaired transition to type A neuroblasts. Our findings indicate that aging of the V-SVZ involves significant non-monotonic changes that are programmed within progenitor cells and are observable independent of the aging niche.

INTRODUCTION

Neurogenesis, the generation of functional neurons from neural progenitor cells (NPCs; which include neural stem cells [NSCs] and more restricted progenitors), occurs throughout life in defined regions of the adult mammalian brain: the dentate gyrus of the hippocampus and the ventricular-subventricular zone (V-SVZ) of the lateral ventricles, from which newborn neurons migrate down the rostral migratory stream (RMS) into the olfactory bulb (OB) (Figure 1A). The V-SVZ is the most proliferative adult neurogenic region in rodents and is an active stem cell niche in humans, although its proliferative potential and ability to produce neurons diminishes dramatically in early postnatal life (Sanai et al., 2011). The adult murine V-SVZ is a highly organized structure, with NPCs interacting with both the ependymal surface and blood vessels (Mirzadeh et al., 2008; Shen et al., 2008; Tavazoie et al., 2008). Quiescent stem cells (type Bq cells) become activated (type Ba cells) and give rise to transit-amplifying type C cells, which in turn generate type A neuroblasts that migrate to the OB (Figures 1A and 1B). Type A cells form chains encased by astrocytes and migrate toward the OB, where they differentiate into specific subtypes of interneurons depending on their anteroposterior and dorsoventral V-SVZ origin (Merkle et al., 2007). These neurons play a role in the structural integrity of the OB and in olfactory memory, fear conditioning, and pheromone-linked behavior (Ming and Song, 2011). In addition, a dedicated type C population gives rise to oligodendrocytes, which primarily migrate to the corpus callosum, striatum, and hippocampal fimbria (Ortega et al., 2013).

Aging is associated with significant declines in NPC function and neurogenesis, which in turn are associated with memory and cognitive impairment (Galvan and Jin, 2007). With age, the cytoarchitecture of the V-SVZ is disrupted; the niche thins, and the lateral ventricle undergoes stenosis, restricting neurogenesis to the anterior dorsolateral aspect (Luo et al., 2006); type A cells are reduced and fewer neurons reach the OB (Luo et al., 2008; Mobley et al., 2014). How these changes evolve with aging is not known, nor whether they depend on signals from the aging niche or are programmed in V-SVZ NPCs. To address these questions, we performed an unbiased analysis of the transcriptome of the whole V-SVZ of male mice over four ages (2, 6, 18, and 22 months) and of the behavior of V-SVZ NPCs *in vivo* and *in vitro* at the clonal level. Our observations indicate that aging in the adult neurogenic niche is a dynamic process that is dominated by non-monotonic changes in gene expression and progenitor behavior that show a reversal of trend centered on the 18-month time point in this four-time-point analysis. Transcriptome analysis highlighted genes expressed in type Ba and type C cells, and we found that *in vivo* there is a decline in the number and division rate of MASH1$^+$ progenitors to 18 months, then a surprising recovery at 22 months, so that there are more MASH1$^+$ cells in the V-SVZ at this age, with a proliferation rate similar to that of young animals. Although there are more MASH1$^+$ cells at 22 months there are fewer type A neuroblasts, suggesting

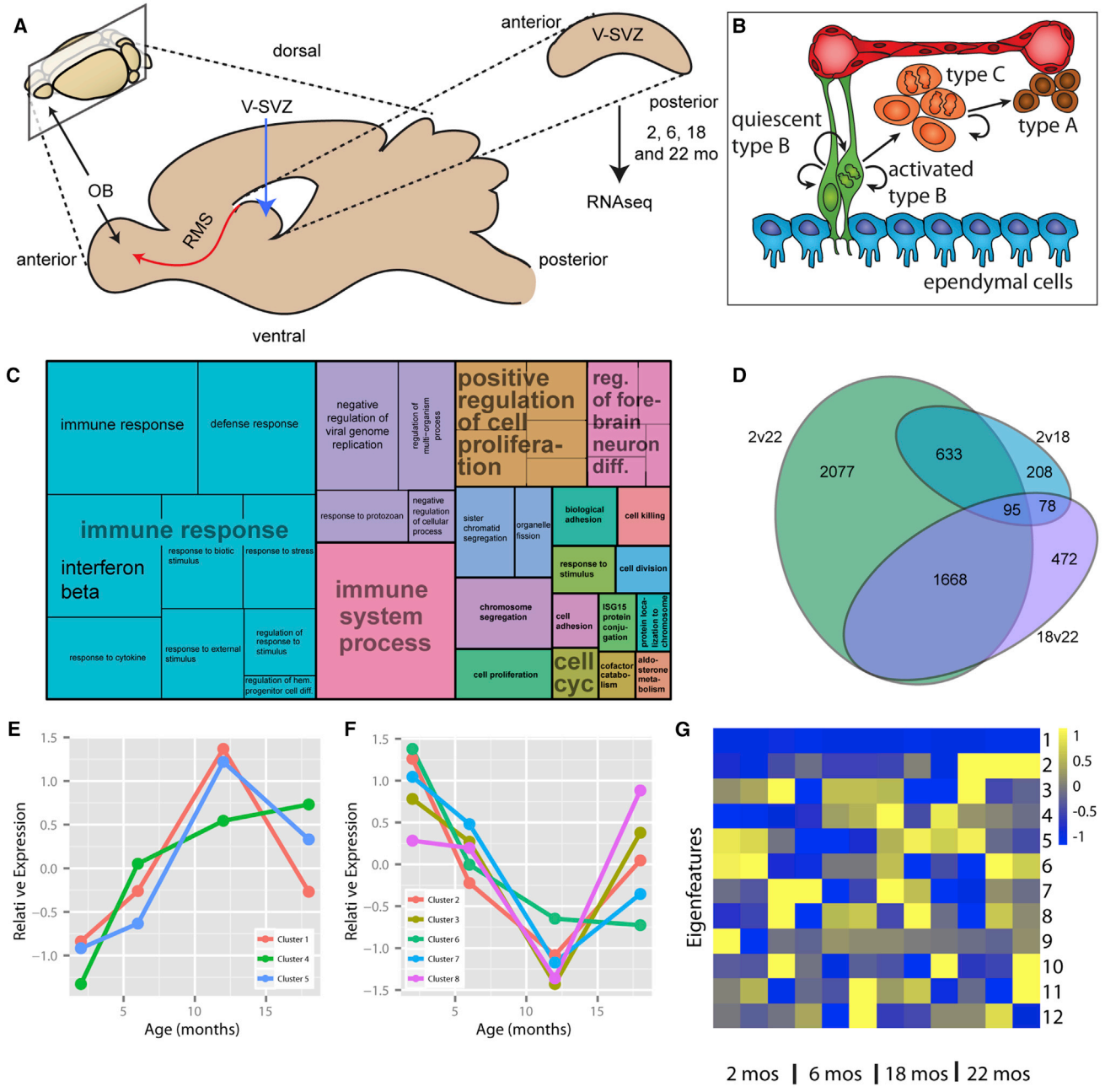

Figure 1. Transcriptomic Analysis of Aging V-SVZ

(A) Schematic of the adult mouse V-SVZ. mo, months old; RMS, rostral migratory stream; OB, olfactory bulb.

(B) Schematic of V-SVZ lineage progression: type B stem cells give rise to transit-amplifying type C cells, which produce type A neuroblasts.

(C) Treemap of enriched GO categories of significantly changing genes.

(D) Significantly changing genes for each pairwise age comparison.

(E and F) Average time course for genes associated with each cluster that increase or decrease with age.

(G) Correlation of each sample with SVD eigenfeatures.

See also Tables S1 and S2.

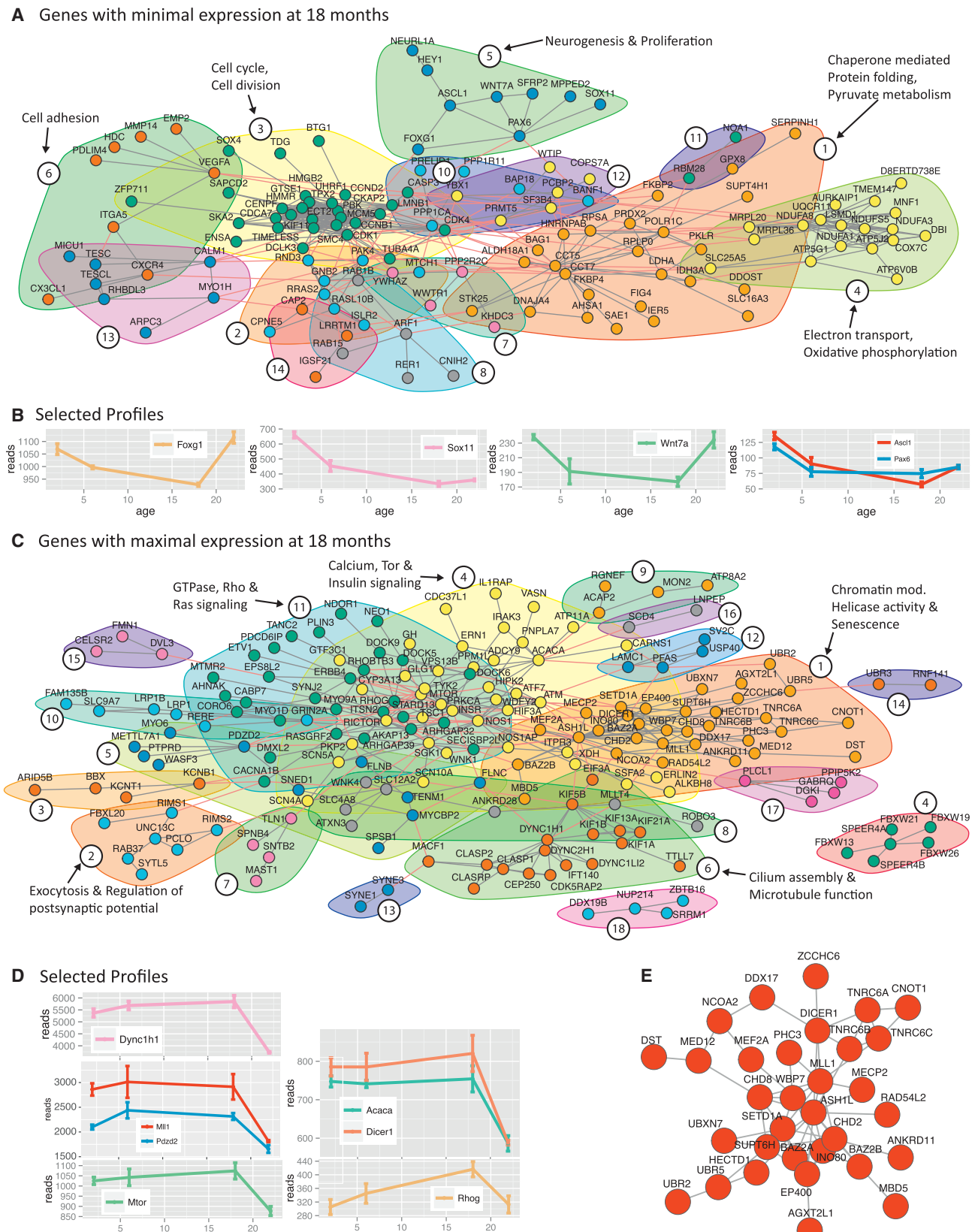

(legend on next page)

an impairment of differentiation. Furthermore, we found that these age-associated changes in progenitor function are mirrored by isolated cells *in vitro*, indicating that programmed changes contribute significantly to the aging process in the adult neurogenic niche.

RESULTS

Global V-SVZ Transcriptome Analysis Reveals Non-monotonic Changes in Gene Expression with Aging

To identify age-associated molecular and signaling pathway dynamics in the adult V-SVZ, we isolated and sequenced RNA from 2-, 6-, 18-, and 22-month-old male mouse V-SVZs (n = 3 animals/age) and identified genes that significantly changed over the time course (Table S1). We identified the enriched gene ontology (GO) categories of the total significantly changing genes, shown in Figure 1C in a tree map, which highlighted genes associated with cell proliferation, forebrain neuron differentiation, and immune responses. Figure 1D shows a Venn diagram of the overlap of these genes in time-point pairwise comparisons, which shows, unexpectedly, that there are more genes with significantly changing expression between the relatively short span of 18–22 months than over the much longer span of 2–18 months.

We then grouped significantly changing genes by fuzzy c-means clustering based on similarity in their temporal expression patterns (Figures 1E and 1F; Table S2). Of the total significantly changing genes, 11% and 10% had monotonic decreased or increased expression, respectively with advanced age, while 37% and 42% showed a maximum or minimum of expression, respectively, at 18 months, i.e., most are non-monotonic. Hence, surprisingly, over these four ages there is evidence of a significant reversal of trend in V-SVZ gene expression between 6 and 22 months. This is reflected in the second component of the singular value decomposition (SVD) analysis as an explicit behavior that is anti-correlated with the first three ages and positively correlated with the 22-month samples (Figure 1G, second row). This analysis identified 292 genes with highest expression at 18 months (max genes), and 226 with lowest expression at 18 months (min genes) (Table S3). Comparison of these genes against a database of type Bq versus type Ba cell transcriptomes (Codega et al., 2014) shows that genes upregulated in Ba cells (compared with Bq) are more likely to be min genes, and play a role in cell proliferation, while those upregulated in Bq cells (compared with Ba) are more likely to be max genes and play a role in differentiation processes (Figure S1A).

There was notable network connectivity within the max and min gene sets (Table S4; Figures 2A and 2C). Prominent genes and pathways in min gene subnetworks are those involved in cell cycle, cell adhesion, metabolism, and chaperone-mediated protein folding (neighborhood numbers 3, 6, and 1, respectively). We note that the neurogenesis and proliferation neighborhood includes genes known to be expressed in type Ba and type C cells: *Sox11*, *Mash1* (*Ascl1*), and *Pax6* (Figures 2A, 2B, and S1B) (Brill et al., 2008; Codega et al., 2014; Moraga et al., 2015). *Foxg1* is also in this neighborhood, and we found a substantial overlap by immunostaining of FOXG1 with MASH1, which is expressed in type C cells and a subset of type Ba cells (Kim et al., 2011) (Figure S1C). *Pax6* connects to *Banf1* in neighborhood 10, and this gene is also enriched in type Ba cells (Codega et al., 2014). The max gene networks include neighborhoods (numbers 4 and 1, respectively) involved in calcium, mTor, and insulin signaling, chromatin modification, helicase activity, and senescence (Figures 2C–2E). One of the central genes in the latter neighborhood is the chromatin remodeling factor *Mll1*, which is expressed in type C cells and regulates their differentiation into type A progeny (Lim et al., 2009). These observations suggest that genes affecting type Ba/type C cell proliferation and differentiation contribute to non-monotonic changes in V-SVZ aging.

In Vivo Analysis Reveals Minima in MASH1$^+$ Progenitor Prevalence and Proliferation at 18 Months

The major classes of V-SVZ progenitor cells, type B, C, and A cells, express *GFAP*, *Mash1*, and *Dcx*, respectively, in both young and aging mice (Luo et al., 2006, 2008; Moraga et al., 2015) (Figure S2). In the transcriptome analysis, *Dcx* shows a monotonic decline with age, but *Mash1* shows a minimum at 18 months when comparing the four ages. To determine whether the expression of *Dcx* and *Mash1* correlates with NPC subtype abundance, we cut and stained coronal sections from male mice aged 2, 18, and 22 months for DCX or MASH1 and quantified these as described in

Figure 2. Network Analysis and Expression Profiles of Max and Min Genes

(A and C) Network constructed from min and max genes, respectively, with neighborhoods colored: gray lines connect within a neighborhood, red lines connect between neighborhoods; some neighborhoods are labeled with associated enrichment categories.

(B) Gene expression time courses for selected min genes associated with the neurogenesis and proliferation neighborhood.

(D) Gene expression time courses for selected max genes from multiple neighborhoods.

(E) Network max neighborhood (#1) associated with chromatin modification.

See also Figure S1; Tables S3 and S4.

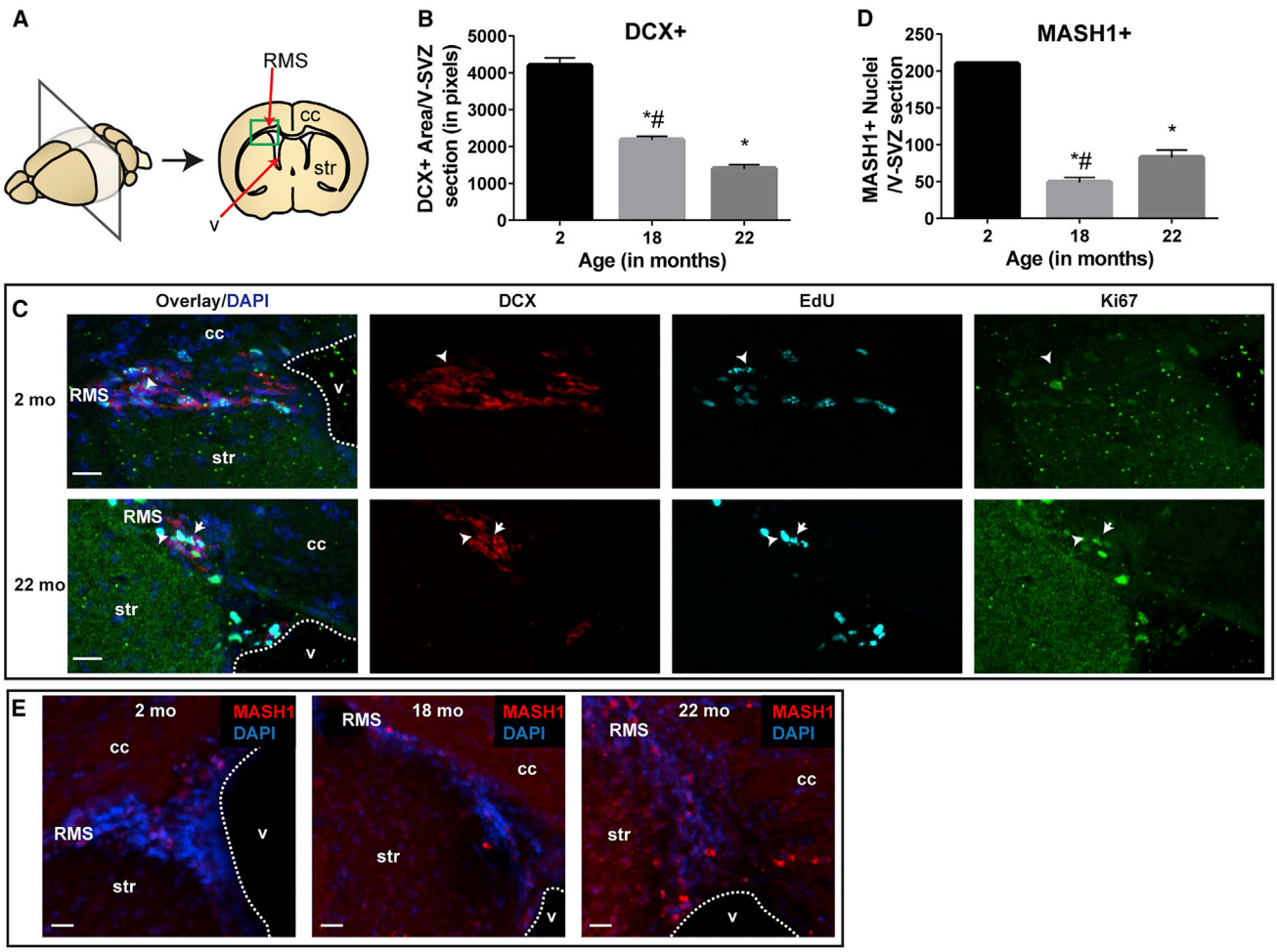

Figure 3. DCX$^+$ and MASH1$^+$ Cell Numbers Follow *Dcx* and *Mash1* Expression with Age

(A) Schematic of mouse brain coronal sections; square indicates where images were taken.

(B) The V-SVZ area (in pixels) positive for DCX was lower for 18 and 22 months (n = 3–6 mice, $p < 0.0001$, one-way ANOVA, post test for linear trend).

(C) Representative fluorescent images of coronal V-SVZ sections from 2- and 22-month-old mouse. Sections were immunostained for DCX (red), EdU (cyan), Ki67 (green), and DAPI (blue). Arrows point to triple-labeled DCX$^+$EdU$^+$Ki67$^+$ cells, while arrowheads indicate double-labeled DCX$^+$EdU$^+$ cells.

(D) Numbers of MASH1$^+$ nuclei were significantly different between all age comparisons, with a reduction at 18 compared with 2 or 22 months (n = 3–6 mice, $p < 0.02$, one-way ANOVA, uncorrected Fisher's least significant difference [LSD]).

(E) Representative images, MASH1 (red) and DAPI (blue).

Graphs show mean ± SEM; * and # indicate that the value is significantly different from 2 and from 22 months, respectively. RGB levels on microscopy images were adjusted as appropriate for visual clarity. cc, corpus callosum; str, striatum; v, ventricle. Dotted line indicates ventricle border. Scale bars, 20 μm. See also Figure S2.

Experimental Procedures (Figure 3A). In agreement with *Dcx* expression levels, young animals had more DCX$^+$ type A cells than older mice (Figures 3B and 3C; $p < 0.05$; n = 3 animals/age). Similarly, in agreement with the *Mash1* min pattern of expression, MASH1$^+$ cell abundance declined between 2 and 18 months but then increased in number between 18 and 22 months (Figures 3D and 3E; $p < 0.05$; n = 3 animals/age).

As the network analysis of min or max genes included proliferation and cell-cycle associations centered on the 18-month time point, we sought to determine whether there were correlated changes in NPC proliferation with age. We injected male mice at 2, 6, 18, and 22 months of age with 5-chloro-2′-deoxyuridine (CldU) to identify dividing cells, and generated brain coronal sections for quantification. We found that the number of CldU$^+$ cells

significantly diminished with advanced age (Figures 4A and 4B; $p < 0.05$; $n = 3$ animals/age), as expected. We then assessed the rate of cell-cycle re-entry at the key ages (2, 18, and 22 months) by injecting male mice with CldU three times, 2 hr apart, followed 19 hr later by injecting with another thymidine analog, iododeoxyuridine (IdU), three times, 2 hr apart. Coronal sections were cut and stained, and we quantified the double-labeled cells as a measure of cell-cycle re-entry (Figures 4B–4D). We found that at 18 months, V-SVZ NPCs re-entered the cell cycle less frequently than either 2- or 22-month NPCs ($p < 0.05$; $n = 3$ animals/age).

To assess the subtype of NPCs responsible, we injected male mice at 2, 18, and 22 months with 5-ethynyl-2′-deoxyuridine (EdU), euthanized them 19 hr later, then stained coronal brain sections for EdU, Ki67, and MASH1 or DCX (Ki67 is present in nuclei during all phases of the cell cycle, but is absent from cells in G_0). The percentage of DCX^+ type A neuroblasts re-entering the cell cycle increased significantly after 2 months (Figures 3C and 4E; $p < 0.05$; $n = 3$–6 animals/age group). In contrast, the percentage of $MASH1^+$ cells that re-entered the cell cycle was lowest at 18 months (Figures 4F and 4G; $p < 0.05$; $n = 3$ animals/age group). The percentage of proliferative $MASH1^+$ cells ($MASH1^+EdU^+/MASH1^+$) decreased significantly after 2 months, but was similar between the older ages. Hence, as indicated from the transcriptome network analysis, these data point to $MASH1^+$ cell proliferation being dysregulated with aging, resulting in a more rapid division cycle and more $MASH1^+$ cells at 22 months than at 18 months.

Age-Related Changes in NPC Behavior Are Recapitulated in V-SVZ Cells Growing in Clonal Culture

To determine whether these dynamic changes in NPC behavior with aging were dependent on the niche or were due to programmed changes in the cells, we performed an unbiased clonal analysis of V-SVZ NPCs growing in a standardized culture environment using time-lapse recording, enabling analysis and comparison of cell-cycle time and the numbers and types of progeny produced by each NPC. V-SVZs derived from 2-, 6-, 18-, and 22-month-old male mice (3 mice/replicate, 3–4 replicates/age) were dissociated into single cells; there were no significant differences in the proportion of type B, C, or A progenitor cells in the starting population at the different ages (not shown). The NPCs were plated at clonal density and recorded by time-lapse microscopy, capturing an image every 5 min for 4 days *in vitro* (DIV). The resulting clones were then fixed and stained to identify the different progeny types, using markers compatible with *in vitro* analysis ($GFAP^+EGFR^-$ for type Bq; $GFAP^+EGFR^+$ for type Ba; $GFAP^-EGFR^+$ for type C; β-tubulin III^+ for type A; $O4^+$ for cells of the oligodendrocyte lineage) (Doetsch et al., 1997; Pastrana et al., 2009). In total, 944 clones were followed; each lineage tree was reconstructed by following an individual progenitor cell over time, with the assistance of the Lineage Editing and Validation (LEVER) software (Winter et al., 2016) that automatically segments individual cells and tracks them through multiple rounds of cell divisions. The final cells of the lineages were matched with staining to identify cell fate. Figure 5A shows examples of two clones and their progression through time, along with the final fluorescence image identifying the cell types produced and the reconstructed lineage tree. Examples of time-lapse videos of single cells producing clones and their lineages are shown in Movie S1.

Using the LEVER software, we calculated the cell cycle (i.e., division time) of individual cells and found that it varied with V-SVZ final NPC type, as observed previously *in vivo* (Doetsch et al., 1997), with NPCs giving rise to type C cells dividing significantly faster than all others regardless of age (Figure S3A; $p < 0.05$; $n = 22$, 933, 220, and 11 for type Ba, type C, type A, and oligodendrocytes, respectively; this calculation was not possible for putative type Bq cells, as these were found only in 2-cell clones); overlaid on this, intriguing age-related differences were observed. As a population, the average cell-cycle time of V-SVZ NPCs gradually increased from 2 to 18 months, but then surprisingly decreased by 22 months to a level faster than that of 2-month NPCs (Figure 5B) (20.8 ± 0.4 hr, 21.4 ± 0.6 hr, 23.9 ± 0.8 hr, and 18.8 ± 0.4 hr; $n = 677$, 243, 144, and 296 cells for 2, 6, 18, and 22 months, respectively; $p < 0.05$). This proliferative behavior was primarily attributable to type C-producing progenitors, as these showed a maximum cell-cycle duration at 18 months, while at 22 months it was similar to that at 2 months, underscoring the dramatic change in NPC behavior around this age (Figure 5C) (17.6 ± 0.3 hr, 19.1 ± 0.5 hr, 22.1 ± 1.2 hr, and 17.6 ± 0.3 hr; $n = 461$, 152, 81, and 239 cells for 2, 6, 18, and 22 months; $p < 0.05$). In contrast, type A-producing progenitors divided faster with aging, and when isolated from 22-month-old mice had an average cell-cycle length significantly shorter than seen in 2-month-old mice (Figure 5D) (27.9 ± 0.7 hr versus 22.7 ± 1.9 hr, $n = 118$ and 23 cells, for 2 versus 22 months, $p < 0.05$). The cell-cycle length of type Ba- and oligodendrocyte-producing progenitors did not differ with age. Interestingly, a comparison of cell-cycle length at each generation of the lineage trees shows that type C-producing NPCs cycle faster with increasing generation number, independent of age (Figure S3B). It is unlikely that the dramatic differences in type C cell cycle between 18 and 22 months are due to selective isolation of

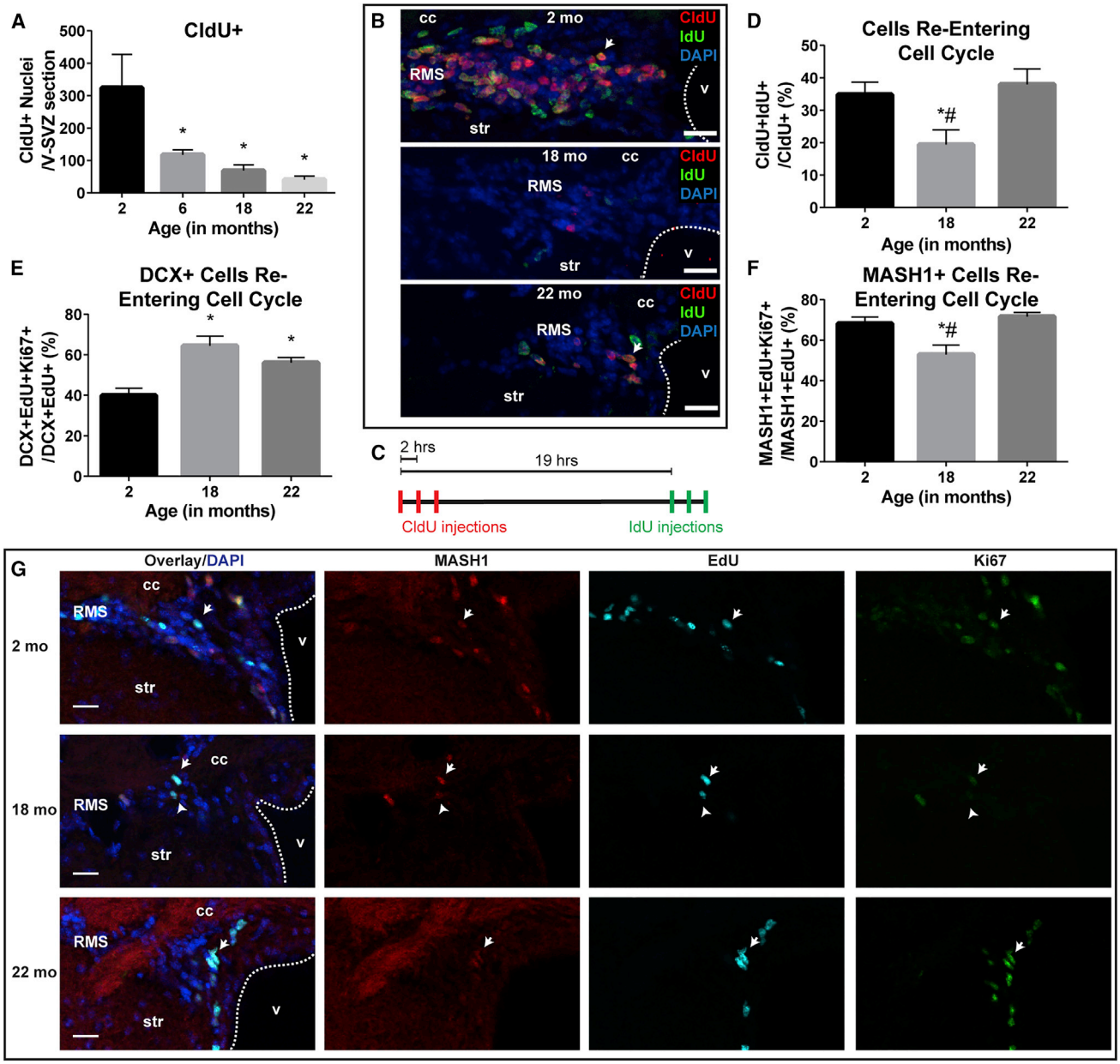

Figure 4. MASH1$^+$ Cells Re-enter the Cell Cycle Less Frequently at 18 versus 2 or 22 Months

(A) Significantly fewer dividing (CldU$^+$) cells at all ages compared with 2 months (n = 3 mice, $p < 0.0003$, one-way ANOVA, post test for linear trend).

(B) Representative images with CldU (red), IdU (green), and DAPI (blue). Arrows point to CldU$^+$IdU$^+$ nuclei.

(C) Schematic of double-labeling experiment.

(D) Significantly fewer cells re-enter the cell cycle at 18 months compared with 2 and 22 months (n = 3 mice, $p < 0.05$, one-way ANOVA, uncorrected Fisher's LSD).

(E) More DCX$^+$ cells re-enter the cell cycle with age compared with 2 months (n = 3–6 mice, $p < 0.03$, one-way ANOVA, post test for linear trend).

(F) Fewer MASH1$^+$ cells re-enter the cell cycle at 18 months compared with 2 or 22 months (n = 3–6 mice, $p < 0.03$, one-way ANOVA, uncorrected Fisher's LSD).

(G) Representative images with MASH1 (red), EdU (cyan), Ki67 (green), and DAPI (blue). Arrows: MASH1$^+$EdU$^+$Ki67$^+$ nuclei; arrowheads: MASH1$^+$EdU$^+$ nuclei.

Graphs show mean ± SEM; * and # indicate that the value is significantly different from 2 and from 22 months, respectively. RGB levels on microscopy images were adjusted as appropriate for visual clarity. Scale bars, 20 μm.

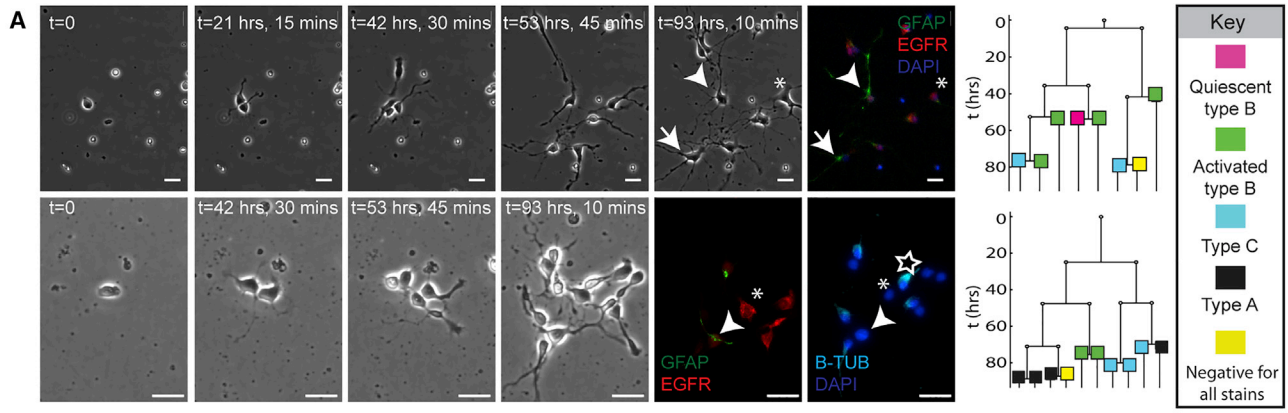

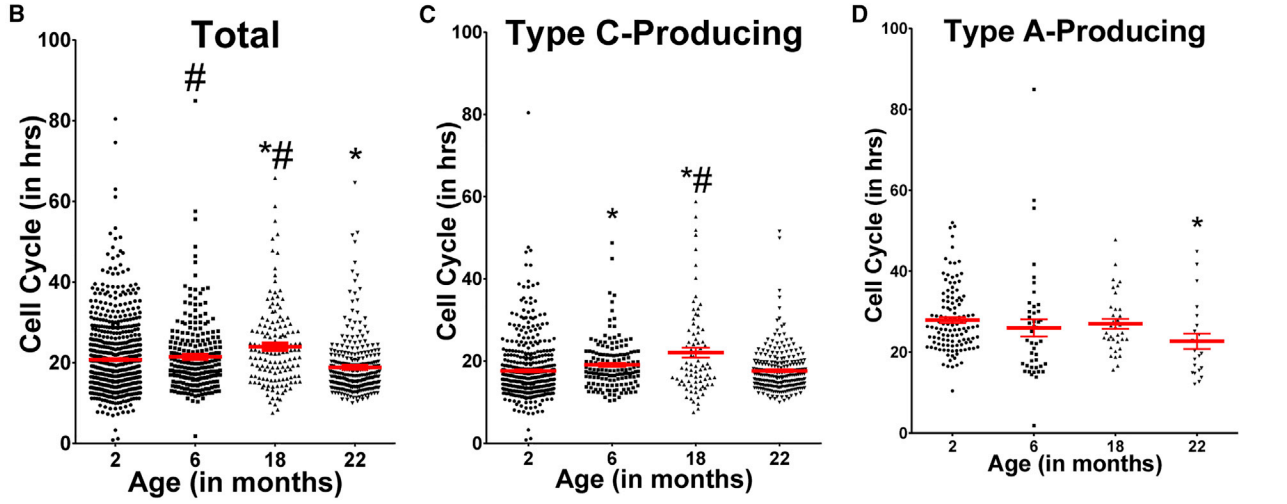

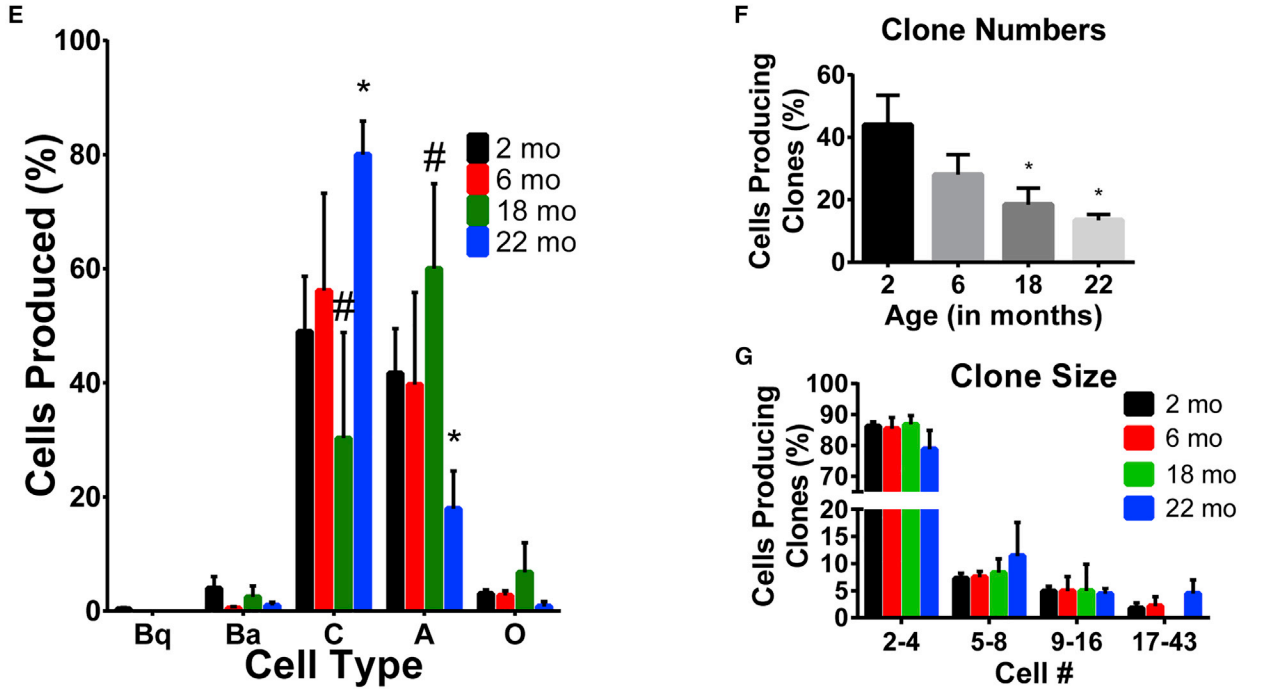

(legend on next page)

neurogenic versus gliogenic type C cells, as oligodendrocyte production did not change with age in clones (Figure 5E), nor does it with aging *in vivo* (Capilla-Gonzalez et al., 2013), and the percentage of $MASH1^+OLIG2^+$ NPCs among total $MASH1^+$ cells is not significantly different between 18 and 22 months (Figure S3C).

Significantly fewer clones were generated at 18 and 22 months compared with 2 months (Figure 5F, $p < 0.05$; n = 3–4). The proportion of clones in each size category did not significantly differ with age, although interestingly while there were no clones in the largest class at 18 months, unexpectedly these were observed at 22 months (Figure 5G). Regarding cell types generated within the clones (Figure 5E), the percentage of type A cells was lowest at 22 months, mirroring the reduced neurogenesis seen *in vivo*. This suggests that even though these progenitors divide faster at older ages, the number of type A-producing progenitors undergoing division is not sufficient to increase the neuroblast population. Oligodendrocyte and type Ba production did not differ between these four ages, while type Bq production was not observed after 2 months. Notably, the proportion of type C cell progeny was greater at 22 months than at 18 months and even than at 2 months ($p < 0.05$; n = 3–4). The proportion of mixed clones (containing both neuronal and glial fates) did not change with age, as shown in Figure 6, a representative summary of different lineage trees generated by NPCs extracted at 2, 6, 18, and 22 months.

Further LEVER-based analyses allowed us to gather data on numerous physical and kinetic characteristics of V-SVZ progenitor cells over time, including cell process area, length, and soma area (Figure 7 and Movie S2). These analyses showed that, unlike type A cells, type C cells show several morphological and dynamic features that exhibit a reversal of trend at 18 months (Figure 7). Specifically, the area surrounding the cell that was occupied by cell processes was almost twice as wide in type C-producing cells at 18 months than at the other ages (Figure 7C). In addition, the primary cell axis (the longer axis of the cell, l in Figure 7A), reached a maximum at 18 months and the cells became slightly more circular (the ratio between the two axes of a cell, l/w in Figure 7A) (Figures 7D and 7E). One notable feature we observed in the time-lapse movies is that the nuclei of type C cells and the NPCs that gave rise to them migrate between the various axes of the cell (Figure 7F and Movie S2) in a manner reminiscent of the intracellular nuclear migration reported for embryonic progenitor cells (Miyata et al., 2015). The nuclear migration of 18-month type C cells and their progenitors was less random than that of the other ages, i.e., the nucleus either favored one of the cell processes to move toward, or its movement was limited overall (Figure 7H). In contrast, the same metrics when examined for type A cells and their progenitors produced monotonic patterns with age. These data further support our conclusion that type C cells and the type Ba cells that give rise to them undergo a significant change in phenotype midway through the aging process. This, combined with the transcriptome data and *in vivo* analysis, leads to the conclusion that non-monotonic changes contribute significantly to the aging of the V-SVZ adult neurogenic niche, and that these changes are in large part programmed within aging NPCs.

Figure 5. Clonal Analysis Reveals that Type C Cells and Their NPCs Show a Proliferative Minimum at 18 Months, while Type A Cells and Their NPCs Divide Faster with Age

(A) Time-lapse stills of two representative clones from 2-month V-SVZ, with final immunostaining and reconstructed lineage trees. Arrows point to putative quiescent type B cell ($GFAP^+$); arrowhead points to activated type B cell ($GFAP^+EGFR^+$); asterisk indicates type C cell ($EGFR^+$); star indicates type A cell (β-tubulin$^+$). Scale bars, 20 μm.

(B) Total NPC cycle significantly lengthened between 2 and 18 months of age, but at 22 months was significantly shorter than at all other ages (n = 144–677 cells).

(C) Type C cells and their progenitors show a maximum cell-cycle length at 18 months, significantly different from that at both 2 and 22 months; the cell cycle significantly slowed between 2 and 6 months (n = 81–461 cells).

(D) Type A cells and their progenitors had significantly shorter cell cycle between 2 and 22 months (n = 23–118 cells).

(E) Clone composition with age; 22-month cells produced more type C cells and fewer type A cells compared with 2 months, without significant differences in other cell products. Bq cells were only observed in 2-month clones. Of the 944 clones, only 3 consisted entirely of type Ba cells (one each from 2-, 6-, and 18-month V-SVZs) (n = 3–4 independent experiments, $p < 0.03$, two-way ANOVA, multiple t tests with a desired false discovery rate of 1%).

(F) A significantly smaller percentage of older (18 and 22 months) V-SVZ cells produced clones compared with 2-month cells (n = 3–4 independent experiments, $p < 0.04$, one-way ANOVA, post test for linear trend).

(G) The percentage of clones in each size category with age; note the lack of large 17–43 clones at 18 months (n = 3–4 independent experiments).

Graphs show individual cell-cycle length means ± SEM, indicated by red in dot plots. $p < 0.05$; one-way ANOVA, Dunn's multiple comparisons test. In (B) to (G), * and # indicate that the value is significantly different from 2 months and 22 months, respectively. RGB levels on microscopy images were adjusted as appropriate for visual clarity. See also Movie S1 and Figure S3.

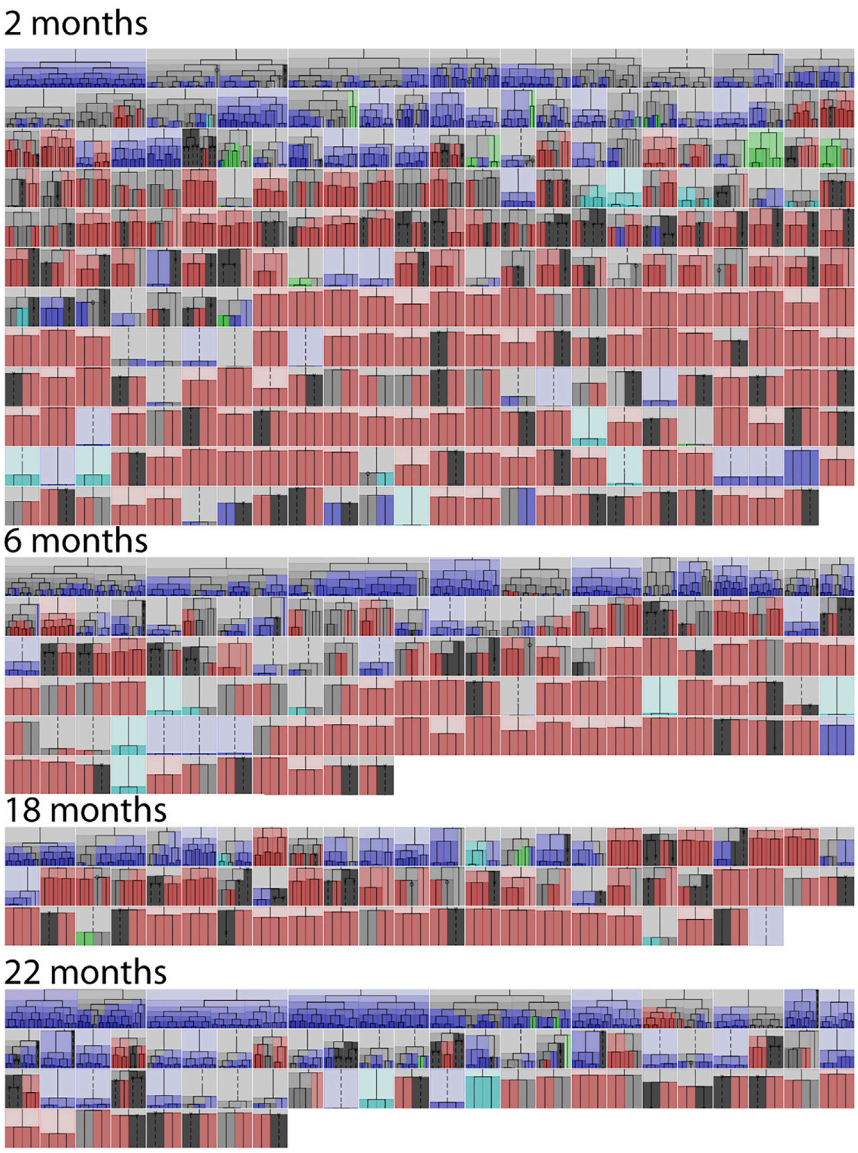

Figure 6. Representative LEVER-Generated Lineages

Lineages are colored according to their final progeny fate: type B (green), type C (blue), type A (red), oligodendrocyte (cyan), and dead (dark gray). Mixed fate junctions in the lineage trees are indicated in light gray. Note the decline in clone size and diversity with age that reaches a minimum at 18 months. Overall, the proportion of asymmetric cell divisions producing daughters of different fates, and corresponding mixed clones, versus uniform clones, did not significantly change with age (mixed clones made up 20%–28% of all the clones). Sixteen clones included type B cells whose progenitors underwent asymmetric divisions (12 from young, and 2 each from 18- and 22-month V-SVZs).

DISCUSSION

While prior studies have demonstrated a dramatic reduction of neurogenesis *in vivo* and have noted a paradoxical increase in the remaining NPC division rate in old animals (Luo et al., 2006, 2008; Shook et al., 2012), the global changes in gene expression in the niche and the time course of these changes has not been fully analyzed. By comparing four ages, we show that while there are changes in the V-SVZ transcriptome that trend up or down with age, unexpectedly most of the significantly changing genes show a reversal of expression trend at 18 months. An unbiased clonal analysis of V-SVZ NPCs shows a decline in type B self-renewal and neurogenesis with age, as reported *in vivo*. Furthermore, clonal analysis shows that type C cells and their progenitors (type Ba cells) exhibit changes in cell cycle, cell morphology, and dynamic behaviors with maxima or minima at the 18-month time point, even after isolation from the niche, and mirroring the abundance and proliferation of MASH1$^+$ cells we found *in vivo*. Together, these data demonstrate that adult NPCs exhibit dynamic, programmed changes, which could contribute to neurogenic decline and the development of age-related disease.

Transcriptome analysis of the V-SVZ at 2, 6, 18, and 22 months identified temporal trends that were monotonic, as expected, but surprisingly, most of the variance was explained by genes with maxima or minima of expression at 18 months. Analysis of the min genes reveals related neighborhoods involved in neurogenesis, proliferation, and cell cycle. A prominent gene in the neurogenesis

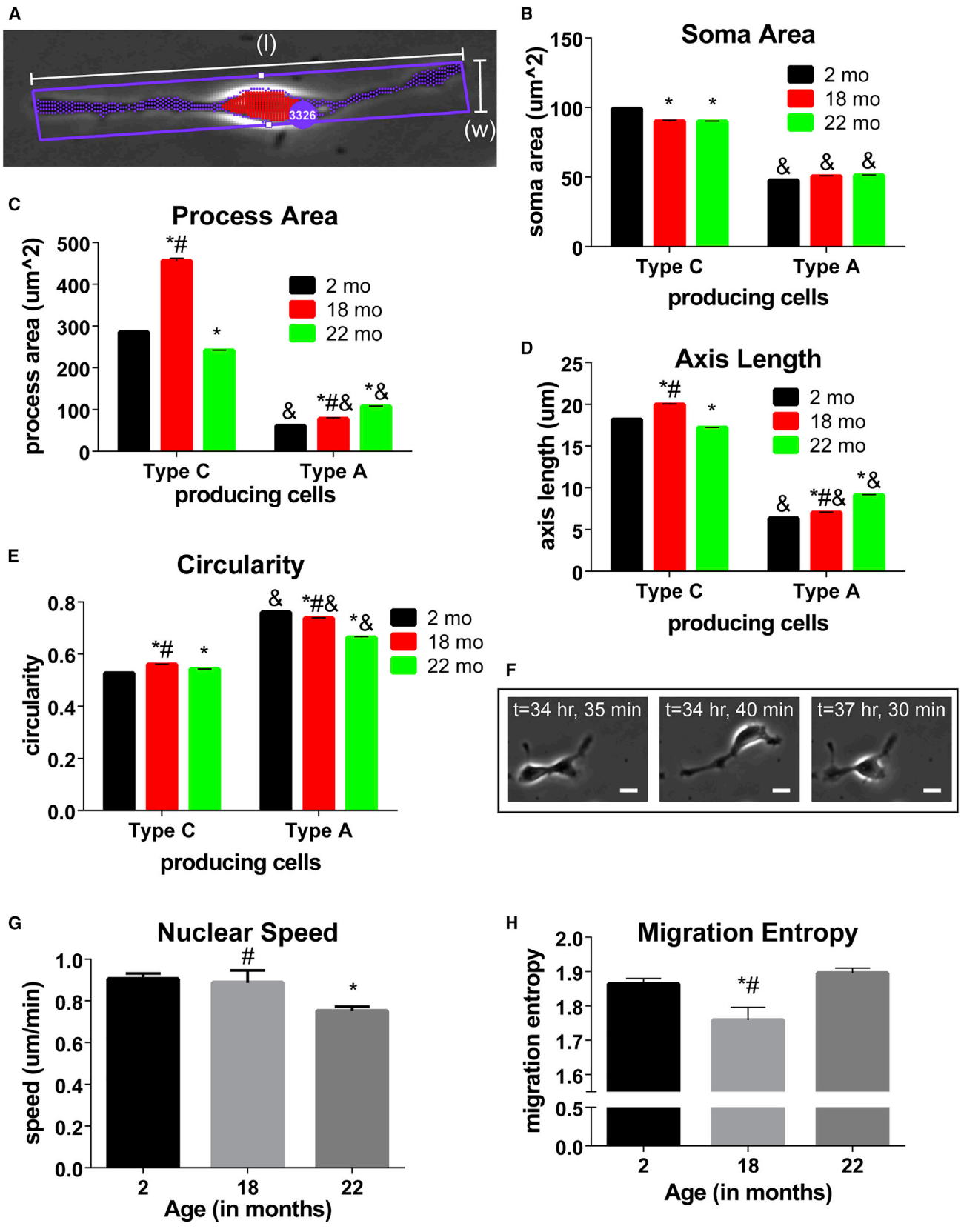

(legend on next page)

neighborhood (#5) is *Ascl1* (*Mash1*), which is expressed in type C and a subset of type Ba cells (Kim et al., 2011). MASH1 regulates genes involved in cell-cycle progression (Kim et al., 2011; Castro et al., 2011), fitting with the observation that type C cells exhibit a reversal in cell-cycle time after 18 months. *Ascl1* connects to *Foxg1*, which we show is expressed in MASH1$^+$ cells, and connects the neurogenesis and proliferation neighborhood to the cell division neighborhood (#5 and #3, respectively). Increased expression of *Foxg1* shortens the cell cycle while reduced expression of *Foxg1* has the opposite effect (Martynoga et al., 2005; Yip et al., 2012); hence, changes in *Foxg1* may be instrumental in the observed change in division rate, along with the prominent group of cell division regulators seen in that min gene neighborhood. Remarkably, while the transcriptome was obtained for the entire V-SVZ, genes associated with production of type C cells emerge from this analysis, indicating that this population has a unique response to aging. The neurogenesis and proliferation neighborhood also includes components of the Wnt signaling pathway. Wnt7a promotes adult NPC proliferation and can be expressed by the NPCs themselves, acting in an autocrine manner (Qu et al., 2010). Hence, changes in the environment produced by NPCs may contribute to the observed age-associated differences. The chromatin binding protein BANF1 appears to have a central role in the min gene network as it connects the electron transport, oxidative phosphorylation, neurogenesis and proliferation, and cell-cycle neighborhoods (#4, #5, and #3, respectively). BANF1 associates with the nuclear envelope and is required for proper nuclear assembly and chromatin organization during cell division (Paquet et al., 2014), and mutations in *Banf1* have been associated with the Nestor-Guillermo progeria syndrome (Cabanillas et al., 2011).

Analysis of the max genes also reveals interesting functional neighborhoods. Neighborhood #4 is enriched in calcium, mTOR, and insulin signaling, all of which have been associated with aging. Another max neighborhood (#1) is associated with chromatin binding, helicase activity, and senescence and includes the chromatin remodeling factor *Mll1*, which plays a key role in V-SVZ neurogenesis (Lim et al., 2009). In *Mll1*-deficient V-SVZ cells, *Ascl1* is maintained but there is impairment of downstream *Dlx2* activation and differentiation into neurons. Reduced Mll1 activity at 22 months could help explain why type C progenitors increase in number while type A cells decrease, possibly due to impairment in lineage progression so that type C cells divide but do not effectively produce type A progeny. Another prominent gene in this neighborhood is *Ash1l*. This encodes a histone methyl transferase that methylates lysine 36 of histone H3 (H3K36me) (An et al., 2011). Interestingly, H3K36me3 marks appear to be involved in suppressing age-dependent changes in the transcriptome, and a reduction in these marks leads to a shortened lifespan (Pu et al., 2015). Thus *Ash1l* reduction at 22 months could contribute to accelerated aging, and the fact that *Ash1l* connects to many other neighborhoods means that it may be a key player in the max gene network.

The percentage of type A neuroblasts generated from single NPCs *in vitro* was markedly reduced with old age, mirroring the dramatic decline in neurogenesis observed *in vivo*. Our data corroborate recent findings (Daynac

Figure 7. Morphometry and Kinetics of Type C and Type A Cells and Their Progenitors *In Vitro*

(A) LEVER algorithms track the soma (red), processes (purple), and overall cell dimensions (represented by the purple rectangle surrounding the cell) over time (Cardenas De La Hoz et al., 2016). This image is a cropped still from a time-lapse series that has been pseudocolored by LEVER for tracking purposes. l, primary cell axis; l/w, circularity.

(B) The soma area of type C cells and their progenitors was significantly smaller at the older ages (18 and 22 months) compared with 2 months, while it was unaffected by age in the case of type A cells and their progenitors.

(C and D) The process area (C) and length (D) of type C cells and their progenitors was maximum at 18 months when compared with 2 and 22 months, with 22-month progenitors showing a significant decrease compared with 2-month progenitors. In the case of type A cells and their progenitors, the soma area and length significantly increased with each advanced age tested.

(E) Cell circularity was measured as the ratio of primary to secondary cell axes. Type C cells and their progenitors were significantly more circular at 18 months compared with 2 and 22 months, with 2-month progenitors being significantly more circular than 22-month progenitors. Type A cells and their progenitors were significantly less circular with each advanced age tested. In all ages, type A cells and their progenitors had significantly smaller somata and fewer extended processes, and were significantly shorter and more circular than type C cells and their progenitors. Two-way ANOVA, Tukey's multiple comparisons test. In (A) to (E), n = 16–216 cells.

(F) An example of nuclear migration. Scale bars, 10 μm.

(G) The speed of nuclear migration of type C cells and their progenitors significantly decreased at 22 months compared with 2 months. One-way ANOVA, post test for linear trend.

(H) Nuclear migration entropy was calculated as a measure of how close to random was the probability of nuclear movement. Type C cells and their progenitors showed a significant minimum in migration entropy, i.e., a more predictable nuclear movement, at 18 months compared with 2 and 22 months. One-way ANOVA, Fisher's uncorrected LSD. In (G) to (H), n = 64–216 cells.

Graphs show means ± SEM; $p < 0.05$. * and # indicate that the value is statistically different from 2 and 22 months, respectively; & indicates that the value for type A cells is significantly different from the value for type C cells at the corresponding age. See also Movie S2.

et al., 2016) that reduced V-SVZ neurogenesis is seen relatively early, within 4–6 months *in vivo*. Luo et al. (2006) reported that more type A cells underwent apoptosis in old versus young mice *in vivo*, while this was not observed in clones *in vitro*, which could reflect a deficit in the aging niche to support type A survival. The fact that only type C production increases in clones with old age, while type A cell production overall significantly decreases (and similarly *in vivo* we found an unexpected increase in MASH1$^+$ cells between 18 and 22 months while type A cell numbers declined), further supports the concept that aging could adversely affect the transition of type C to type A cells. Consistent with this, we observed fewer clones containing both type C and type A cells at 18 and 22 months.

In clonal culture, self-renewing divisions producing putative type Bq were only observed in 2-month NPCs, a finding in accordance with the loss of type B cells reported *in vivo* with aging, and the concept that the NSC population is fixed, with limited self-renewal, so that the NSCs are gradually depleted with age as each is recruited (Encinas et al., 2011; Luo et al., 2006). Of the 944 clones followed, no single progenitor gave rise to both neuroblasts and oligodendrocytes, agreeing with the lack of evidence for common progenitors *in vivo* (Ortega et al., 2013). Furthermore, we found no significant difference in the number of oligodendrocytes generated with age *in vitro*, corroborating *in vivo* findings (Capilla-Gonzalez et al., 2013).

Time-lapse experiments enabled accurate determination of cell-cycle length associated with cell-type-specific progenitors. Type C-producing progenitors were the fastest proliferating cells, while V-SVZ type B NPCs were the slowest, regardless of age. Our observations corroborate *in vivo* data showing that type C cell divisions are more rapid than type B cell divisions (Doetsch et al., 1997), indicating that this is a property programmed into the different cell types. Thus, dynamic features of isolated V-SVZ progenitor cells can be predictive of fate, as observed previously for retinal progenitor cells (Cohen et al., 2010).

Overall, NPC cell cycle lengthened between 2 and 18 months of age and then shortened by 22 months, with old cells cycling even faster than their young counterparts. In accordance, *in vivo* fewer cells re-entered the cell cycle from 2 to 18 months, while the number re-entering at 22 and 2 months was similar. Daynac et al. (2015) reported a lengthening of the cell cycle of V-SVZ NPCs *in vitro* up to 12 months (the oldest age examined), attributable to a longer G_1 phase. A previous study also reported a lengthening of the cell cycle with aging *in vivo*, determined by double labeling with proliferation markers at 2, 10–13, and 19–22 months (Luo et al., 2006); grouping the older animals together might have obscured the later increase in cell-cycle re-entry we observed. Tropepe et al. (1997) reported that fewer V-SVZ NPCs re-entered the cell cycle *in vivo* with advanced age, while Stoll et al. (2011) published the opposite result. The complex temporal behavior we show here might help explain the apparent contradictions between prior reports. The finding that type C cells and their progenitors (type Ba cells) exhibit a dramatic shortening of the cell cycle between 18 and 22 months indicates that these NPC subtypes may be more prone to cell division dysregulation with aging. Our data also suggest that type C and A cells and their progenitors do not undergo typical senescence, but display increased cell-cycle re-entry in old age, with an impairment of lineage progression.

V-SVZ type B and C cells exhibited nuclear migration during the cell cycle while the majority of type A cells did not, regardless of the age of the animal from which they were isolated. Such nuclear motion has been associated with the cell cycle in rodent cortical neurogenesis and in adult avians (Alvarez-Buylla et al., 1998; Miyata et al., 2015), but to our knowledge there has been no prior recording of such movement in adult mammalian NPCs. In the embryo, nuclear migration toward the apical side of the ventricular zone (the embryonic V-SVZ) is required for mitosis and is thought to influence final cell fate (Florio and Huttner, 2014; Reiner et al., 2012). In isolated V-SVZ type B and C cells, the speed of the nucleus decreased with advanced age, but nuclear movement is more directed, i.e., the nucleus was less random in its movements, in 18-month-old animals. It is possible that nuclear movement would permit progenitor cell nuclei to move between differently oriented cell processes and therefore different compartments in the niche, but it remains to be seen whether such motion occurs *in vivo*. These different dynamic behaviors are reflected in changes in type C cell morphology, with maxima in overall process area, axis length, and circularity at 18 months. Why type C cells demonstrate these unique temporal changes in phenotypic properties is an intriguing point that deserves further study, especially into the subnetworks of max and min genes that notably include type C cell regulators, and may contribute to the observed cell behavioral changes. While in our study of four time points the maxima or minima in gene expression and cell behavior were mostly centered at 18 months, a more detailed study of multiple ages will identify more precisely when changes in behavior occur, and could reveal more complex patterns of temporal changes. It should also be noted that different survival rates at the ages examined could influence outcome, since male C57BL/6 mice survival at the vendor facility is reported to be 90% at 19 months and 75% at 24 months (online NIA resources). Although no 18- to 22-month-old males died at our facility, we do not know the death rate during this period at the vendor facility. Therefore, it is possible that survivorship contributed to the observed reversal of trend, instead of the trend being reflective of phenotypic changes during aging. These possibilities could be distinguished by

longitudinal studies, which will be a point for future investigations.

To reduce cohort effects, i.e., the impact of shared experience, we designed experiments wherever possible to use animals obtained from different cohorts (details are provided in Experimental Procedures). For example, the time-lapse experiments were conducted on animals obtained over a period of more than 1 year, with multiple ages examined per experiment, after which the data from different cohorts were combined. For one experiment, the CIdU/IdU immunolabeling to assess cell-cycle re-entry, all animals were obtained in a single order, but the findings were supported by subsequent EdU-labeling experiments obtained from animals in different cohorts.

To counteract the loss of neurogenesis *in vivo* with aging, revitalization studies typically seek to increase NPC markers and cell proliferation. However, as seen from our study, these parameters may also be associated with advanced aging and are therefore not secure indicators of NPC rejuvenation. Other measures that might be valuable in such studies are an increase in clonal frequency and an increase in neuron production. Furthermore, the transcriptional impact of regenerative protocols should be evaluated to determine whether genes that show strong correlation with sample age demonstrate the desired recovery.

The fact that several features associated with V-SVZ aging *in vivo*, including the decline in neurogenesis, are seen in clones growing in a standardized environment indicates that NPCs themselves are aging, although changes in the niche could contribute to the development of such differences. These findings focus attention on the programmed transitions that adult neurogenic stem cells and their progeny undergo with age, and a deeper understanding of these will be valuable in counteracting aging effects. Furthermore, this study indicates that there might be particular points within the aging process that should be targeted to slow down or prevent age-related declines in NPC activity and neurogenesis.

EXPERIMENTAL PROCEDURES

Detailed information is provided in Supplementary Experimental Procedures.

Animals

All animal work was performed under the supervision of the Institutional Animal Care and Use Committee at SUNY Albany, license number 14-011.

Animals used were male wild-type *a/a* C57BL/6 mice and were ordered as close as possible to the intended age of use.

Animals were euthanized by isoflurane inhalation, and their SVZs dissected and dissociated to single cells as previously described (Kokovay et al., 2012).

RNA Isolation

V-SVZ RNA was isolated using TRIzol, from three animals per age category. Isolated RNA was sent for RNA sequencing.

In Vivo Cell-Cycle Comparisons and Section Immunostaining

For $CldU^+IdU^+$ double labeling, three mice per age category were injected intraperitoneally with 50 mg/kg CldU three times, 2 hr apart. Nineteen hours after each CIdU injection, animals were injected with 50 mg/kg IdU (three IdU injections in total). Twenty-four hours after the last injection, animals were transcardially perfused with a 4% formaldehyde solution while under the effects of 0.15 cc of a 390 mg/mL solution of Beuthanasia-D.

Brains where then removed and immersed in a 30% sucrose solution and then in OCT (optimum cutting temperature) compound, and frozen. Coronal sections of the V-SVZ, 40 μm thick, were cut from approximately 1.94 mm to −0.1 mm in relation to bregma. Every second or third section from a single animal was used for each replicate (6–9 sections/replicate). Sections underwent antigen retrieval by being boiled with 10 mM citrate buffer (pH 6) for 15 min, then incubated with 2 M HCl for 30 min at room temperature, and subsequently washed twice with 0.1 M borate buffer (pH 8.5) for 5 min at room temperature. Sections were permeabilized with 0.5% Triton X-100 for 1 hr at room temperature and then blocked with 10% donkey serum in permeabilization buffer for 1 hr at room temperature. Sections were stained sequentially with anti-CldU (1:50; overnight at 4°C), then anti-IdU (1:250; 2 hr at RT), then DAPI (1:1,000; for 10 min at room temperature).

Secondary antibodies used were Alexa 568 and 488 and were applied at 1:300 overnight at 4°C. Images of the entire V-SVZ were taken for both V-SVZs of each section. All nuclei in the V-SVZ that were $CldU^+$ alone were counted.

For other experiments, 3–6 mice per age category were injected intraperitoneally with 50 mg/kg EdU and euthanized after 19 hr as described above. Coronal brain sections, 18 or 40 μm thick, were used (5–9 sections/replicate) and blocked as already described, and stained with anti-DCX (1:300; overnight at 4°C) or anti-MASH1, the EdU kit according to the manufacturer's specifications, anti-Ki67 (1:200; over two nights at 4°C), and DAPI (as mentioned above). Images were taken as described above. The DCX^+ area in the entire V-SVZ section (both V-SVZs of each section) was measured. $MASH1^+$ cells, and cells double- or triple-stained for Ki67, DCX, or MASH1, and EdU in the entire V-SVZ section (both V-SVZs of each section), were counted.

In all cases, counts were blinded and means were generated for each mouse brain first and then compared between the animals of each age group.

All sections used in the same experiment (regardless of age) were stained contemporaneously and imaged using the same microscope settings. RGB levels on presented microscopy images were adjusted as appropriate for visual clarity.

Cell Culture, Time-Lapse Microscopy of V-SVZ Cell Clones, and LEVER Analysis

Single V-SVZ cell suspensions were acquired from three mice per experimental replicate and plated as described in Kokovay et al. (2012) with a few modifications. Growth medium was DMEM,

supplemented with 1 mM Na-pyruvate, 2 mM L-glutamine, 0.16 μg/mL N-acetyl-L-cysteine, N-2 supplement, B-27 supplement, 0.01 μg/mL fibroblast growth factor 2, 0.01 μg/mL brain-derived neurotrophic factor, 0.05 μg/mL NRG1, 0.1 mM QVD, and 0.01 mM Y27632. Cells were allowed to settle for 2 hr before medium was changed to remove tissue debris. Cells were re-fed once at day 2 after isolation and experiments were ended at 4 DIV.

Plates were imaged in an environmental chamber at 37°C and 5% CO_2. For each replicate, nine fields of vision with cells were chosen randomly from four wells per age group, totaling 36 fields/age group/replicate. Fields were imaged every 5 min before cells were fixed and immunostained as described below. Three to four experimental replicates were performed for each age group.

Cells were fixed with 5% paraformaldehyde in PHEM buffer (pH 6.9) (120 mM PIPES, 50 mM HEPES, 20 mM EGTA, and 8 mM $MgCl_2.6H_2O$) for 20 min at room temperature. Cells were then stained sequentially for O4 (for 45 min at room temperature) and EGFR (overnight at 4°C). Cells were then permeabilized with 0.1% Triton X-100 and sequentially stained for GFAP (for 45–60 min at room temperature), after which the first set of images was taken. Cells were then stained for β-tubulin III (for 45–60 min at room temperature) and DAPI (for 5 min at room temperature), and the final set of images was taken. Primary antibodies used were an O4 hybridoma produced in-house, anti-EGFR (at 1:200), anti-GFAP (at 1:400), and anti-β-tubulin III (at 1:500). Secondary antibodies used were Alexa 647, 546, and 488. Cells were stained with secondary antibodies for 20–30 min at room temperature. Images were taken using a Zeiss Axiovert D1 microscope. Means were generated first for each replicate and then compared between the replicates in each age group. RGB levels on presented microscopy images were adjusted as appropriate for visual clarity.

Lineage trees were created using the LEVER delineation and tracking algorithms.

Bioinformatics, Linear Data Fitting, and Statistics

Processing of RNA sequencing data and subsequent analysis utilized the R statistical language and the EdgeR and DeSeq packages (Robinson et al., 2009). Global data analysis was performed by Pearson correlation. SVD (Alter et al., 2000) was employed to determine major contributions to variation in the data and to numerically describe the relationship of the samples to each other. We used fuzzy c-means clustering (Kumar and Futschik, 2007) to group significantly changing genes based on similarity between their temporal expression patterns. Fuzzy clustering was conducted using the Mfuzz Bioconductor package for R. SVD was computed using the BioSVD Bioconductor package for R. We used GOSeq to identify the enriched GO categories of the total significantly changing genes. Treemaps were constructed using REVIGO. Max and min genes were termed as genes that did the following: (a) exhibited significant differences in expression between at least three pairs of time points and (b) had maximum or minimum expression at 18 months (confirmed by a comparison of a linear fit for the first three time points and a linear fit for the final two time points). The first criterion was relaxed for genes showing significant differences between only two time points, if those were 2–18 or 6–18 and 18–22. Gene connectivity data were extracted from the String Database (Szklarczyk et al., 2014) using confidence networks that integrate a variety of evidence of connectivity (direct interaction, co-localization, gene regulation, and co-citation) into a single combined score. Gene set enrichment analysis was conducted using the EnrichR application (Chen et al., 2013) allowing comparison of our data against gene sets in KEGG, BioCarta, WikiPathways, Reactome, Gene Ontology, Mouse Brain Atlas, and the Allen Brain Atlas. The iGraph package (Csárdi and Nepusz, 2006) was utilized within the R statistical language to analyze the networks of max and min genes, respectively. Network neighborhoods were identified using the igraph implementations of random walk and edge-betweenness algorithms.

Linear model fits were conducted using the built-in R method "lm()," which conducts a QR decomposition.

For bioinformatics analysis, Fisher's exact test was utilized and false discovery rate corrected $p < 0.05$ used to determine if there were significant changes between samples associated with each possible pair of time points. Measures of significance were conducted in the R statistical language using the DeSeq and EdgeR packages. For all other measurements, statistical analyses (see figure legends) were performed using GraphPad Prism 6.

ACCESSION NUMBERS

The RNA sequencing data have been deposited in the Gene Expression Omnibus (http://www.ncbi.nlm.nih.gov/geo) under accession number GEO: GSE104651.

SUPPLEMENTAL INFORMATION

Supplemental Information includes Supplemental Experimental Procedures, three figures, four tables, and two movies and can be found with this article online at https://doi.org/10.1016/j.stemcr.2017.10.005.

AUTHOR CONTRIBUTIONS

Conceptualization, M.A., A.R.C., and S.T.; Methodology, M.A., T.R.K., and S.T.; Software, T.R.K., M.W., E.C.d.l.H., and A.R.C.; Validation, M.A. and M.W.; Formal Analysis, M.A., T.R.K., M.W., N.C.B., K.L.Z., and E.C.d.l.H.; Investigation, M.A., S.K.G., C.S.B., and Y.W.; Resources, A.R.C. and S.T.; Data Curation, M.A., T.R.K., M.W., E.C.d.l.H., A.R.C., and S.T.; Writing – Original Draft, M.A., T.R.K., and M.W.; Writing – Review and Editing, M.A., T.R.K., M.W., A.R.C., and S.T.; Visualization, M.A., T.R.K., N.C.B., C.S.B., and M.W.; Supervision, A.R.C. and S.T.; Project Administration, A.R.C. and S.T.; Funding Acquisition, A.R.C. and S.T.

ACKNOWLEDGMENTS

We thank Steven Lotz at the Neural Stem Cell Institute Neuracell core facility; Ashlyn DiRisio, Meryl Lindsay, and David Clarkson for lineage tree verification; Kevin O'Keefe and Fiona Doetsch for comments on the manuscript; and Jane Johnson for the MASH1 antibody. This work was supported by NIA (5R01AG041861-03) and the Ellison Medical Foundation (AG-SS-2655-11), as well as NYSTEM (C-029158) support for Neuracell. Opinions expressed here are solely those of the authors and do not necessarily reflect those of the Empire State Stem Cell Board, the New York State Department of Health, or the State of New York.

Received: June 20, 2017
Revised: October 10, 2017
Accepted: October 11, 2017
Published: November 9, 2017

REFERENCES

Alter, O., Brown, P.O., and Botstein, D. (2000). Singular value decomposition for genome-wide expression data processing and modeling. Proc. Natl. Acad. Sci. USA *97*, 10101–10106.

Alvarez-Buylla, A., García-Verdugo, J.M., Mateo, A.S., and Merchant-Larios, H. (1998). Primary neural precursors and intermitotic nuclear migration in the ventricular zone of adult canaries. J. Neurosci. *18*, 1020–1037.

An, S., Yeo, K.J., Jeon, Y.H., and Song, J.J. (2011). Crystal structure of the human histone methyltransferase ASH1L catalytic domain and its implications for the regulatory mechanism. J. Biol. Chem. *286*, 8369–8374.

Brill, M.S., Snapyan, M., Wohlfrom, H., Ninkovic, J., Jawerka, M., Mastick, G.S., Ashery-Padan, R., Saghatelyan, A., Berninger, B., and Götz, M. (2008). A dlx2- and pax6-dependent transcriptional code for periglomerular neuron specification in the adult olfactory bulb. J. Neurosci. *28*, 6439–6452.

Cabanillas, R., Cadinanos, J., Villameytide, J.A., Perez, M., Longo, J., Richard, J.M., Alvarez, R., Duran, N.S., Illan, R., Gonzalez, D.J., et al. (2011). Nestor-Guillermo progeria syndrome: a novel premature aging condition with early onset and chronic development caused by BANF1 mutations. Am. J. Med. Genet. A *155A*, 2617–2625.

Capilla-Gonzalez, V., Cebrian-Silla, A., Guerrero-Cazares, H., Garcia-Verdugo, J.M., and Quinones-Hinojosa, A. (2013). The generation of oligodendroglial cells is preserved in the rostral migratory stream during aging. Front. Cell. Neurosci. *7*, 147.

Cardenas De La Hoz, E., Winter, M.R., Apostolopoulou, M., Temple, S., and Cohen, A.R. (2016). Measuring process dynamics and nuclear migration for clones of neural progenitor cells. Comput. Vis. ECCV *9913*, 291–305.

Castro, D.S., Martynoga, B., Parras, C., Ramesh, V., Pacary, E., Johnston, C., Drechsel, D., Lebel-Potter, M., Garcia, L.G., Hunt, C., et al. (2011). A novel function of the proneural factor Ascl1 in progenitor proliferation identified by genome-wide characterization of its targets. Genes Dev. *25*, 930–945.

Chen, E.Y., Tan, C.M., Kou, Y., Duan, Q., Wang, Z., Meirelles, G.V., Clark, N.R., and Ma'ayan, A. (2013). Enrichr: interactive and collaborative HTML5 gene list enrichment analysis tool. BMC Bioinformatics *14*, 128.

Codega, P., Silva-Vargas, V., Paul, A., Maldonado-Soto, A.R., Deleo, A.M., Pastrana, E., and Doetsch, F. (2014). Prospective identification and purification of quiescent adult neural stem cells from their in vivo niche. Neuron *82*, 545–559.

Cohen, A.R., Gomes, F.L., Roysam, B., and Cayouette, M. (2010). Computational prediction of neural progenitor cell fates. Nat. Methods *7*, 213–218.

Csárdi, G., and Nepusz, T. (2006). The igraph software package for complex network research. InterJournal Complex Syst. *1695*, 1695.

Daynac, M., Morizur, L., Kortulewski, T., Gauthier, L.R., Ruat, M., Mouthon, M.A., and Boussin, F.D. (2015). Cell sorting of neural stem and progenitor cells from the adult mouse subventricular zone and live-imaging of their cell cycle dynamics. J. Vis. Exp. https://doi.org/10.3791/53247.

Daynac, M., Morizur, L., Chicheportiche, A., Mouthon, M.A., and Boussin, F.D. (2016). Age-related neurogenesis decline in the subventricular zone is associated with specific cell cycle regulation changes in activated neural stem cells. Sci. Rep. *6*, 21505.

Doetsch, F., Garcia-Verdugo, J.M., and Alvarez-Buylla, A. (1997). Cellular composition and three-dimensional organization of the subventricular germinal zone in the adult mammalian brain. J. Neurosci. *17*, 5046–5061.

Encinas, J.M., Michurina, T.V., Peunova, N., Park, J.-H., Tordo, J., Peterson, D.A., Fishell, G., Koulakov, A., and Enikolopov, G. (2011). Division-coupled astrocytic differentiation and age-related depletion of neural stem cells in the adult hippocampus. Cell Stem Cell *8*, 566–579.

Florio, M., and Huttner, W.B. (2014). Neural progenitors, neurogenesis and the evolution of the neocortex. Development *141*, 2182–2194.

Galvan, V., and Jin, K. (2007). Neurogenesis in the aging brain. Clin. Interv. Aging *2*, 605–610.

Kim, E.J., Ables, J.L., Dickel, L.K., Eisch, A.J., and Johnson, J.E. (2011). Ascl1 (Mash1) defines cells with long-term neurogenic potential in subgranular and subventricular zones in adult mouse brain. PLoS One *6*, e18472.

Kokovay, E., Wang, Y., Kusek, G., Wurster, R., Lederman, P., Lowry, N., Shen, Q., and Temple, S. (2012). VCAM1 is essential to maintain the structure of the SVZ niche and acts as an environmental sensor to regulate SVZ lineage progression. Cell Stem Cell *11*, 220–230.

Kumar, L., and Futschik, M.E. (2007). Mfuzz: a software package for soft clustering of microarray data. Bioinformation *2*, 5–7.

Lim, D.A., Huang, Y.C., Swigut, T., Mirick, A.L., Garcia-Verdugo, J.M., Wysocka, J., Ernst, P., and Alvarez-Buylla, A. (2009). Chromatin remodelling factor Mll1 is essential for neurogenesis from postnatal neural stem cells. Nature *458*, 529–533.

Luo, J., Daniels, S.B., Lennington, J.B., Notti, R.Q., and Conover, J.C. (2006). The aging neurogenic subventricular zone. Aging Cell *5*, 139–152.

Luo, J., Shook, B.A., Daniels, S.B., and Conover, J.C. (2008). Subventricular zone-mediated ependyma repair in the adult mammalian brain. J. Neurosci. *28*, 3804–3813.

Martynoga, B., Morrison, H., Price, D.J., and Mason, J.O. (2005). Foxg1 is required for specification of ventral telencephalon and region-specific regulation of dorsal telencephalic precursor proliferation and apoptosis. Dev. Biol. *283*, 113–127.

Merkle, F.T., Mirzadeh, Z., and Alvarez-Buylla, A. (2007). Mosaic organization of neural stem cells in the adult brain. Science *317*, 381–384.

Ming, G.L., and Song, H. (2011). Adult neurogenesis in the mammalian brain: significant answers and significant questions. Neuron *70*, 687–702.

Mirzadeh, Z., Merkle, F.T., Soriano-navarro, M., García-, J.M., and Alvarez-buylla, A. (2008). Neural stem cells confer unique pinwheel architecture to the ventricular surface in neurogenic regions of the adult brain. Cell Stem Cell *3*, 265–278.

Miyata, T., Okamoto, M., Shinoda, T., and Kawaguchi, A. (2015). Interkinetic nuclear migration generates and opposes ventricular-zone crowding: insight into tissue mechanics. Front. Cell. Neurosci. *8*, 473.

Mobley, A.S., Rodriguez-Gil, D.J., Imamura, F., and Greer, C.A. (2014). Aging in the olfactory system. Trends Neurosci. *37*, 77–84.

Moraga, A., Pradillo, J.M., Garcia-Culebras, A., Palma-Tortosa, S., Ballesteros, I., Hernandez-Jimenez, M., Moro, M.A., and Lizasoain, I. (2015). Aging increases microglial proliferation, delays cell migration, and decreases cortical neurogenesis after focal cerebral ischemia. J. Neuroinflammation *12*, 87.

Ortega, F., Gascon, S., Masserdotti, G., Deshpande, A., Simon, C., Fischer, J., Dimou, L., Chichung Lie, D., Schroeder, T., and Berninger, B. (2013). Oligodendrogliogenic and neurogenic adult subependymal zone neural stem cells constitute distinct lineages and exhibit differential responsiveness to Wnt signalling. Nat. Cell Biol. *15*, 602–613.

Paquet, N., Box, J.K., Ashton, N.W., Suraweera, A., Croft, L.V., Urquhart, A.J., Bolderson, E., Zhang, S.D., O'Byrne, K.J., and Richard, D.J. (2014). Nestor-Guillermo progeria syndrome: a biochemical insight into barrier-to-autointegration factor 1, alanine 12 threonine mutation. BMC Mol. Biol. *15*, 27.

Pastrana, E., Cheng, L.-C., and Doetsch, F. (2009). Simultaneous prospective purification of adult subventricular zone neural stem cells and their progeny. Proc. Natl. Acad. Sci. USA *106*, 6387–6392.

Pu, M., Ni, Z., Wang, M., Wang, X., Wood, J.G., Helfand, S.L., Yu, H., and Lee, S.S. (2015). Trimethylation of Lys36 on H3 restricts gene expression change during aging and impacts life span. Genes Dev. *29*, 718–731.

Qu, Q., Sun, G., Li, W., Yang, S., Ye, P., Zhao, C., Yu, R.T., Gage, F.H., Evans, R.M., and Shi, Y. (2010). Orphan nuclear receptor TLX activates Wnt/beta-catenin signalling to stimulate neural stem cell proliferation and self-renewal. Nat. Cell Biol. *12*, 31–40, sup pp 1–9.

Reiner, O., Sapir, T., and Gerlitz, G. (2012). Interkinetic nuclear movement in the ventricular zone of the cortex. J. Mol. Neurosci. *46*, 516–526.

Robinson, M.D., McCarthy, D.J., and Smyth, G.K. (2009). edgeR: a Bioconductor package for differential expression analysis of digital gene expression data. Bioinformatics *26*, 139–140.

Sanai, N., Nguyen, T., Ihrie, R.A., Mirzadeh, Z., Tsai, H., Wong, M., Gupta, N., Berger, M.S., Huang, E., Rowitch, D.H., et al. (2011). Corridors of migrating neurons in human brain and their decline during infancy. Nature *478*, 382–386.

Shen, Q., Wang, Y., Kokovay, E., Lin, G., Chuang, S.-M., Goderie, S.K., Roysam, B., and Temple, S. (2008). Adult SVZ stem cells lie in a vascular niche: a quantitative analysis of niche cell-cell interactions. Cell Stem Cell *3*, 289–300.

Shook, B.A., Manz, D.H., Peters, J.J., Kang, S., and Conover, J.C. (2012). Spatiotemporal changes to the subventricular zone stem cell pool through aging. J. Neurosci. *32*, 6947–6956.

Stoll, E.A., Habibi, B.A., Mikheev, A.M., Lasiene, J., Massey, S.C., Swanson, K.R., Rostomily, R.C., and Horner, P.J. (2011). Increased re-entry into cell cycle mitigates age-related neurogenic decline in the murine subventricular zone. Stem Cells *29*, 2005–2017.

Szklarczyk, D., Franceschini, A., Wyder, S., Forslund, K., Heller, D., Huerta-Cepas, J., Simonovic, M., Roth, A., Santos, A., Tsafou, K.P., et al. (2014). STRING v10: protein-protein interaction networks, integrated over the tree of life. Nucleic Acids Res. *43*, D447–D452.

Tavazoie, M., Van der Veken, L., Silva-Vargas, V., Louissaint, M., Colonna, L., Zaidi, B., Garcia-Verdugo, J.M., and Doetsch, F. (2008). A specialized vascular niche for adult neural stem cells. Cell Stem Cell *3*, 279–288.

Tropepe, V., Craig, C.G., Morshead, C.M., and van der Kooy, D. (1997). Transforming growth factor-alpha null and senescent mice show decreased neural progenitor cell proliferation in the forebrain subependyma. J. Neurosci. *17*, 7850–7859.

Winter, M., Mankowski, W., Wait, E., Temple, S., and Cohen, A.R. (2016). LEVER: software tools for segmentation, tracking and lineaging of proliferating cells. Bioinformatics *32*, 3530–3531.

Yip, D.J., Corcoran, C.P., Alvarez-Saavedra, M., DeMaria, A., Rennick, S., Mears, A.J., Rudnicki, M.A., Messier, C., and Picketts, D.J. (2012). Snf2l regulates Foxg1-dependent progenitor cell expansion in the developing brain. Dev. Cell *22*, 871–878.